ICAS 2021 SHANG HAI
International Council of the Aeronautical Sciences
32nd Congress of the International Council of the Aeronautical Sciences
September 6-10, 2021
Pudong Shangri-La, Shanghai, China

A Novel Detect-and-Avoid Approach for UAS in Urban Environments

Suraj Bijjahalli[1], Alessandro Gardi[1], Samuel Hilton[1], Roberto Sabatini[2]

[1]School of Engineering, Aerospace Engineering and Aviation, RMIT University, Australia

[2] Dept. of Aerospace Engineering, Khalifa University of Science and Technology, PO Box 127788, Abu Dhabi, UAE

Corresponding author: roberto.sabatini@ku.ac.ae

Abstract

This paper addresses one of the key contemporary issues in avionics and Air Traffic Management (ATM) systems research: the development of a certifiable Detect-and-Avoid (DAA) system for trusted autonomous Unmanned Aircraft System (UAS) operations. DAA systems for unmanned aircraft are required to achieve a level of safety that is at least equivalent to the see-and-avoid capabilities of their manned counterparts. To achieve this overarching goal, DAA systems must account for the uncertainty arising from a number of different sources within the available Separation Assurance and Collision Avoidance functionalities. This paper proposes a novel approach to UAS DAA which accounts for the performance of the Communication, Navigation and Surveillance (CNS) systems, as well as a number of dynamic factors impacting the likelihood of a collision. The methodology is underpinned by rigorous modelling of the CNS performance characteristics, and the translation of those characteristics to the spatial domain to form a dynamic (i.e., performance-driven) geo-fence around each aircraft or ground obstacle track. Inflations are then applied to the volume to account for factors such as relative platform dynamics, uncertainty in wind forecasts, wake turbulence and adverse weather conditions. The methodology is demonstrated through case studies involving the use of Primary Surveillance Radar (PSR) and ADS-B to detect intruder aircraft.

Keywords: UAS, avionics, navigation, ATM, detect and avoid, DAA, RNP, RCP, RSP, ADS-B, radar, CNS performance, separation assurance, d collision avoidance.

1. Introduction

The current airspace is in a state of transition owing to the ongoing introduction of Unmanned Aircraft System (UAS) operations in the existing airspace. The UAS Traffic Management (UTM) concept [1] is envisaged as a means of safely and efficiently integrating and managing unmanned traffic. At a fundamental level, the basic UTM concept is a cooperative network which is separate from, but complementary to Air Traffic Management (ATM) separation services and based primarily on the sharing of information between operators on flight intent and airspace constraints. Apart from unmanned aircraft, the emergence of on-demand Urban Air Mobility (UAM) will also place increasing demands on the airspace. As UAM and UTM operations scale in size, transitions of conventional air traffic and unmanned aircraft across UAM corridors will have to be accounted for and managed. The management of the airspace and operations require the use of metrics or safety indices that characterize the airspace. These metrics are used to assess the safety of ongoing operations as well as the impact of proposed changes to operations. Consequently, evaluation of the metric(s) against safety thresholds are used to trigger remedial actions to avoid safety hazards. Traditionally, the probability of aircraft collision or collision risk, or alternatively, conflict risk has been widely used in conventional ATM processes as a safety metric to assess operations and to trigger remedial actions to avoid hazards. Since air-air/air-ground collisions are the primary hazards associated with

unmanned aircraft operations, this metric is well-suited to drive airspace management in the different timeframes of a UAS operation. The relevant operational timeframes are adapted from manned aircraft [2] to the UAS context and are illustrated in Figure 1. Offline conflict evaluations are applicable before the mission commences i.e., when the aircraft is on the ground. During the online phase, while the mission is in progress, conflict assessment is performed over aircraft intents spanning multiple sectors (strategic) or within one sector (tactical).

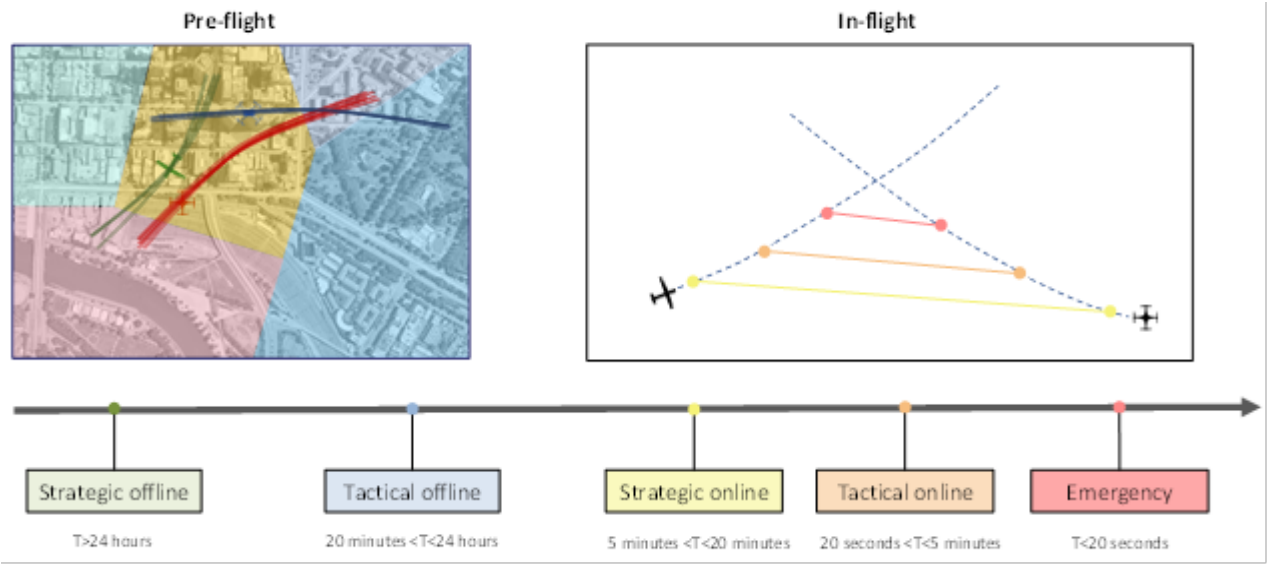

Figure 1 - Operational timeframes for UAS missions.

Within the tactical online and emergency timeframes, DAA robustness is crucial in ensuring that aircraft can self-separate with the likelihood of collision maintained below a designated (extremely low) threshold. The typical sequence of events in assessing the likelihood of a collision is as follows. At any given epoch, the own (host) aircraft and intruder aircraft states are estimated. The uncertainty in these estimates depend on the employed sensors, their update rates, and fusion algorithms. Depending on whether a cooperative or non-cooperative surveillance modality is employed, the state information may or may not be shared between aircraft. These states are then propagated over a time horizon using known, assumed or estimated dynamic and/or kinematic models of the own and intruder aircraft. Knowledge of perturbations can be incorporated in the propagation such as model-forecasts of wind and other weather phenomena. At each iteration of the time horizon, a set of metrics are evaluated to check for a collision. Different metrics are used in the literature. A common practice is to explicitly evaluate the probability of collision or collision risk. Alternatively, metrics that are surrogates for collision risk can also be used. These include the estimated time and distance to closest point of approach assuming constant velocities and headings.

This paper proposes a unified approach to DAA (suitable for both cooperative/non-cooperative scenarios) which accounts for the performance of Communication, Navigation and Surveillance (CNS) systems of the aircraft involved in the encounter, in addition to weather phenomena and wake turbulence. A new analytical approach is presented to translate these factors to buffer layers that jointly form a dynamic geofence around each aircraft or ground/human-made obstacles (e.g., in low-level flight operations).

Section 2 briefly presents prior work in this domain. Section 3 presents the overview of the methodology followed by its mathematical underpinnings. Section 4 demonstrates the generation of each buffer layer as a function of CNS performance. Section 5 presents the simulation case studies and the demonstration scenarios.

2. Prior work

Most prior work in this application area is captured in the review of Conflict Detection and Resolution (CD&R) methods by Kuchar and Yang [3] (up to 2000), and subsequently, in the review by Tang [4] (up to 2019). The methodologies in the literature are primarily differentiated by the state propagation method, as well as the sources of uncertainty that are considered. Aircraft positioning errors are typically considered with suitable worst-case assumptions made regarding the navigation and surveillance equipment. Host and intruder aircraft uncertainties are typically combined using rotational transformations to a common coordinate system. An often-used methodology for this is provided in [5]. State propagation methods typically fall into one of three categories [3]: Nominal, worst-case, and probabilistic. Most methods either employ nominal propagation methods with the inclusion of safety buffers [6], or probabilistic approaches [5]. Worst-case propagation methods are less frequently employed owing to the propensity for a high false alarm rate. In time-propagating the states, it is necessary to account for the impact of the wind on the predicted relative positions of the aircraft. The frequency and accuracy of wind forecasting tools has steadily increased over the decades. However, wind forecasts are subject to uncertainty which must be accounted for during the propagation stage of conflict prediction. In [7], a stochastic wind field model is used to describe the wind over the propagation interval. Subsequently, a simulation-based approach is adopted wherein multiple trajectories are propagated to derive a probabilistic reach set. A conflict is predicted if the reach sets of two or more aircraft intersect. In addition to wind uncertainty, it is also necessary to account for uncertainty arising from system performance, mainly the performance of the Communication, Navigation and Surveillance (CNS) systems used in the encounter. However, accounting for all these variables on unmanned aircraft with Size, Weight, Power and Cost (SWaP-C) constraints is challenging owing to the limited onboard computational resources. As a result, much of the research on conflict detection for unmanned aircraft employ surrogate metrics rather than the explicit collision risk. A large body of research on the UAS Detect-and-Avoid (DAA) problem does not explicitly evaluate the risk as a function of the actual probability of collision. Rather, a set of DAA metrics and thresholds are defined that serve as proxy variables for defining a collision. For instance, the Minimum Operational Performance Standards (MOPS) for DAA systems [8] defines time- and distance-based metrics (tau, modified tau, DMOD) and thresholds for issuing caution and warning alerts to initiate avoidance manoeuvres. This framework was extended in [9], where a methodology for assuring the integrity and continuity of estimating these metrics was presented.

3. Model overview

The degradation in CNS performance propagates to the downstream systems such as guidance, control and surveillance (in cooperative surveillance modalities such as ADS-B). Accurate, precise, and reliable navigation is a prerequisite for autonomous Separation Assurance (SA) and Collision Avoidance (CA). This is particularly true for Beyond Visual Line of Sight (BVLOS) operations where the remote pilot cannot visually assess the likelihood of loss of separation from other aircraft or the ground/terrain features. A similar dependency is present in the case of cooperative-surveillance scenarios, wherein state estimates of aircraft are shared across a network to assess and respond to collision threats in a timely manner. The relevant modules in a DAA system are shown in the architecture illustrated in Figure 2. The DAA system (airborne in this instance) receives inputs from the navigation and surveillance systems to estimate the relative distance between the host aircraft and a detected intruder aircraft or obstacle.

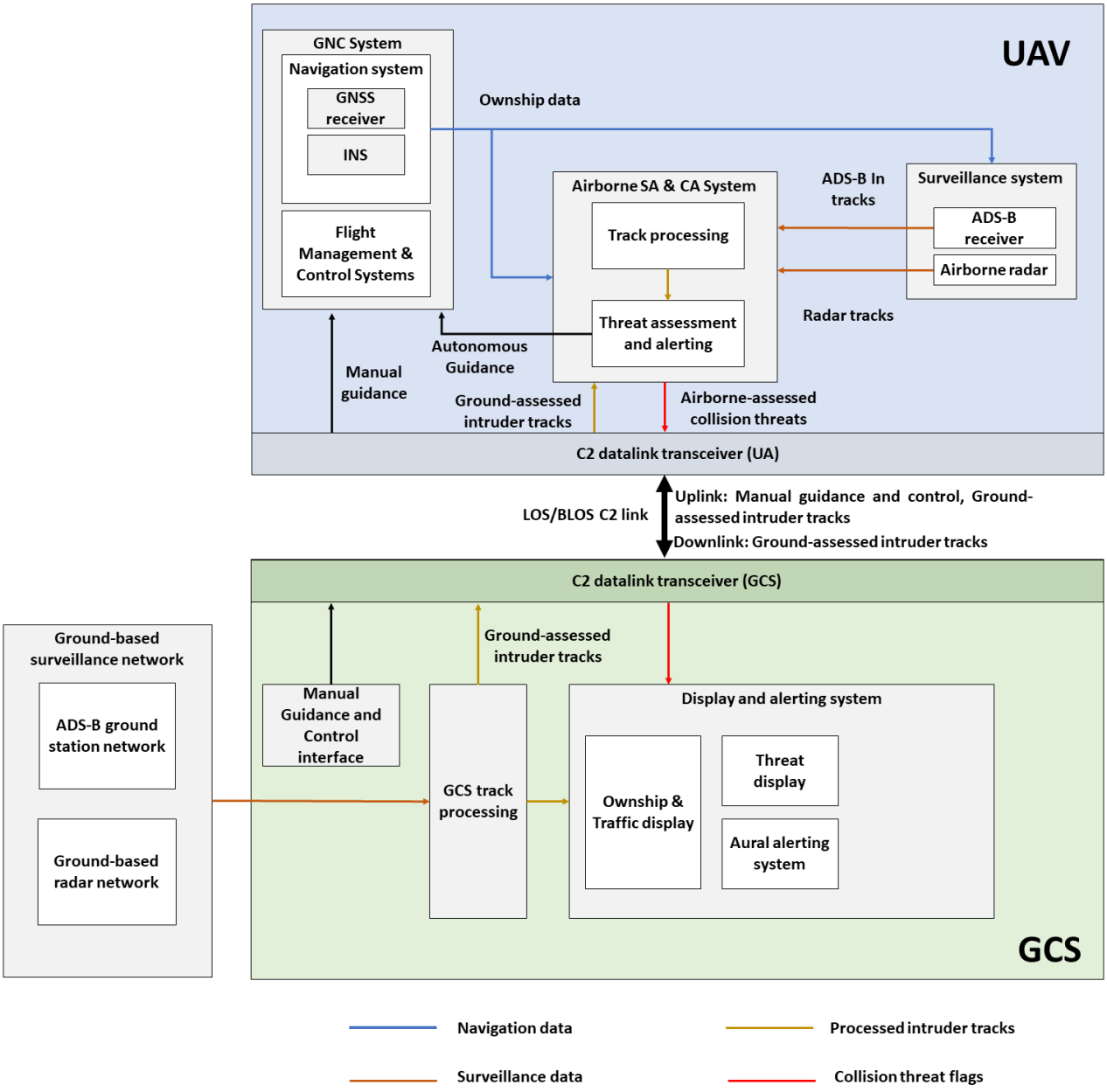

Figure 2 - Functional architecture for SA & CA

An erroneous navigation estimate can ultimately lead to a collision threat flag being issued late or not at all, increasing the likelihood of a collision. Performance degradation, e.g., a loss of accuracy or integrity in navigation, surveillance and communication must, therefore, be captured in DAA systems. In essence, the cause of a collision can be traced back to a failure of the overall CNS+A infrastructure, namely:

- Failure of Navigation systems - Loss of accuracy beyond a specified limit without timely detection. This constitutes hazardously misleading information preventing timely redressal action from remote pilots;
- Failure of surveillance systems - Loss in accuracy of intruder aircraft localization and non-timely relay of surveillance information to downstream sub-systems for recovery actions;

- Failure of Communication - Loss/degradation of link to the point where necessary recovery actions cannot be implemented in a timely manner;

Our proposed approach is to characterize the uncertainty in these performance factors and translate them to a virtual volume or dynamic geofence around each aircraft. This is conceptually illustrated in Figure 4 for a host and intruder aircraft involved in an encounter.

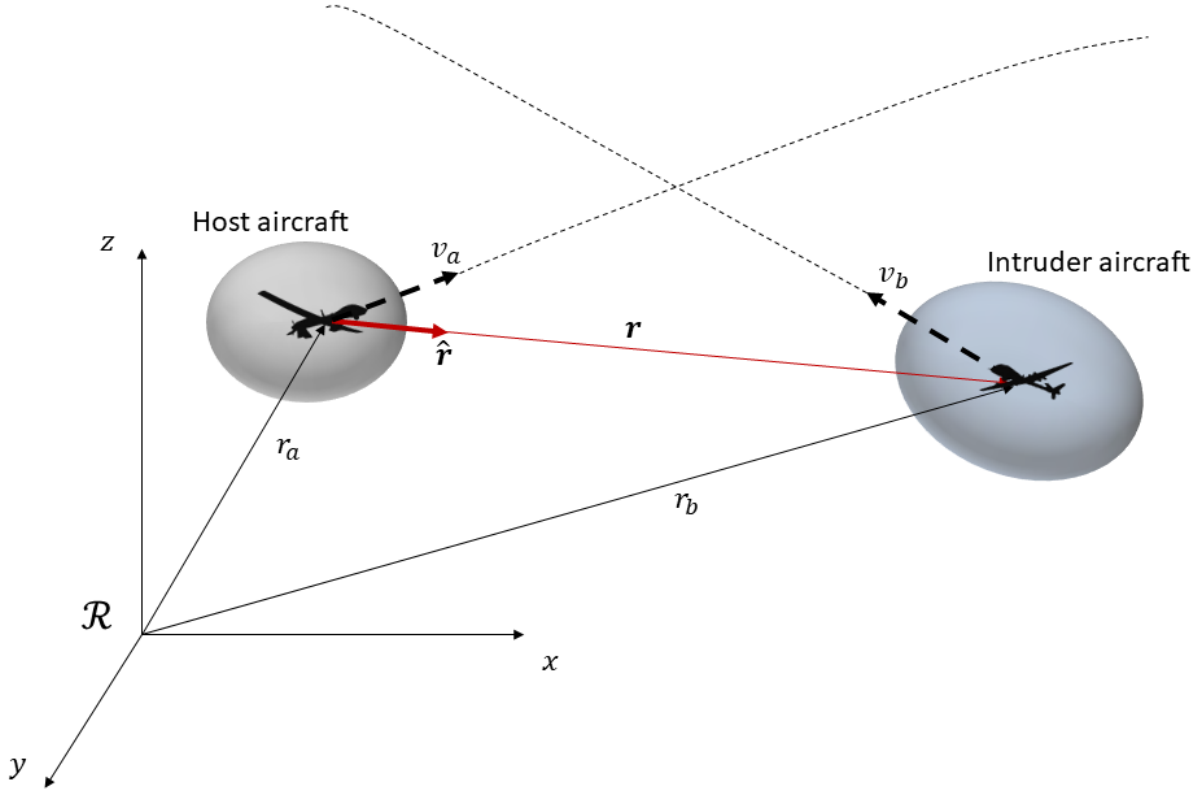

Figure 3 - Scenario representing an encounter between two aircraft.

The errors in aircraft positions and velocities are assumed to follow a Gaussian distribution. This is in line with the de-facto standard for navigation and surveillance systems in aviation. Gaussian distributions are widely used since they provide a relatively simple means of characterizing uncertainty in system states (aircraft states are characterized by a mean and standard deviation). For completeness, the basic formulation of a multi-variate Gaussian probability density function is presented here. Let $\mathcal{N}_n(\xi, \eta, P)$ represent a normal distribution for an n-dimensional variable ξ with mean η and covariance matrix P, i.e

$$\mathcal{N}_n(\xi, \eta, P) = \frac{1}{\sqrt{(2\pi)^n}} \frac{1}{\sqrt{|P|}} exp\left[-\frac{1}{2}(\xi - \eta)^T P^{-1}(\xi - \eta)\right] \quad (1)$$

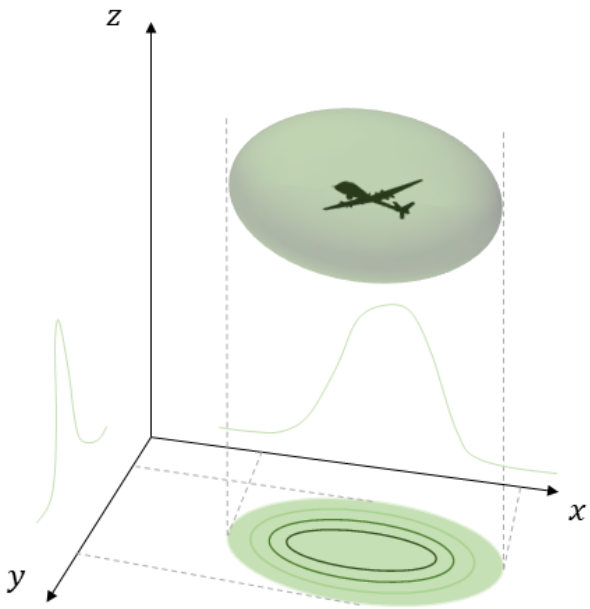

Figure 4 - Uncertainty volume emerging as a result of the multi-dimensional probability density functions.

As an example, Figure 3 shows the aircraft positioning error modelled as a Gaussian random variable with three dimensions. A 3D Gaussian is represented by an ellipsoid. Its projection onto a two-dimensional plane is an ellipse. Under the Gaussian assumption, the motion of each aircraft is characterized by a six-dimensional vector (position and velocity). For the host aircraft, the states as estimated by the navigation system is distributed according to:

$$\rho_a(x_a, t; t_0) = \mathcal{N}_6(x_a, \mu_a, P_a) \tag{2}$$

The intruder aircraft is perceived through a set of surveillance sensors. The corresponding state estimated of the intruder aircraft are distributed according to:

$$\rho_b(x_b, t; t_0) = \mathcal{N}_6(x_b, \mu_b, P_b) \tag{3}$$

with mean μ_a, μ_b and covariance P_a, P_b. In order to construct the dynamic geofence around each intruder aircraft in the scenario, the navigation uncertainty of the host aircraft is first centered on the nominal position of the intruder and then combined with the uncertainty of the intruder position (as estimated by the surveillance sensors). This process is illustrated in Figure 5.

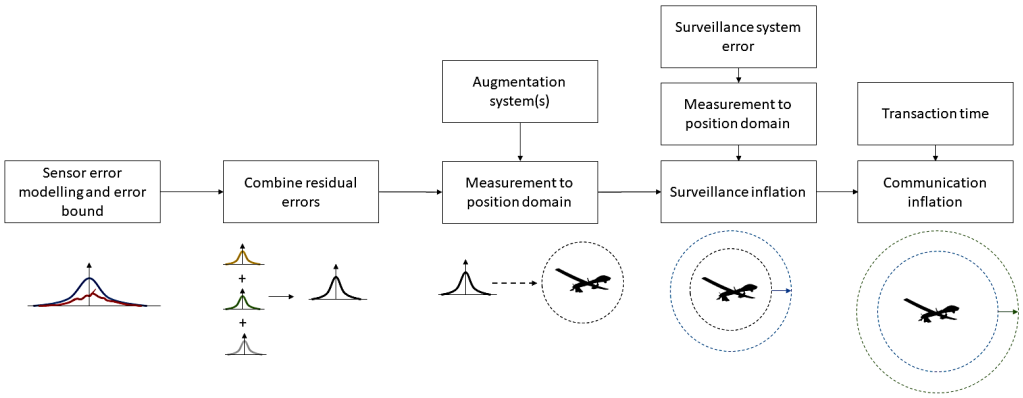

Figure 5 - Process to generate the dynamic geofences.

Navigation sensors are characterized through a modelling effort to capture the distribution of measurement errors which cause aircraft position errors to deviate from nominal fault-free performance. Each error source is represented by a Gaussian distribution carefully chosen so as to conservatively bound the true underlying distribution of the error i.e. each error distribution is replaced by a Gaussian distribution that is ensured to capture the worst-case performance. The rationale for this overbounding process is presented in the next sub-section. The residual error from each error source is combined and the resulting Gaussian distribution is a conservative error budget of the sensor measurements. The conservative sensor errors are then translated from the sensor measurement domain to the aircraft position domain resulting in a volume around the true aircraft position. The dynamic geofence at a given epoch is illustrated in Figure 6 with the navigation and surveillance layers, and a buffer for wind. Further buffers can be added to the volume to account for additional failure modes potentially leading to a collision. A wind buffer layer accounting for the uncertainty in the wind forecast over the trajectory propagation horizon is also illustrated in the diagram. In this manner, each system failure mode is translated to a spatial bound to form the overall risk protection volume. Three sources of uncertainty are covered in this paper – navigation, surveillance and wind forecasts. Each of these sources of uncertainty are described in turn.

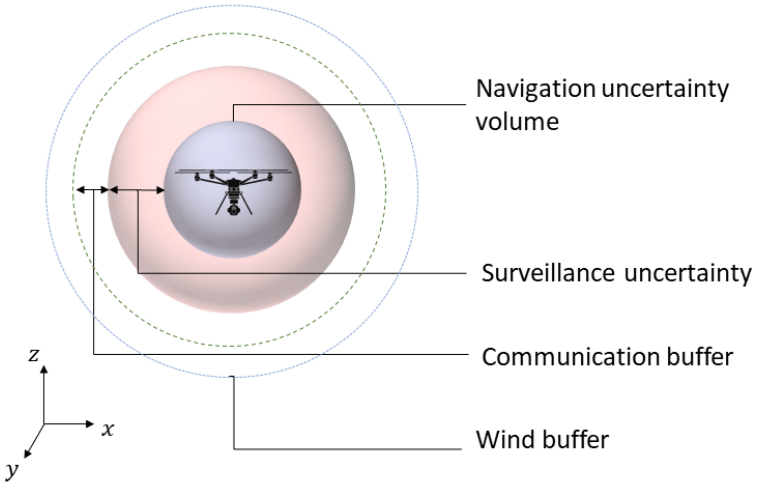

Figure 6 - Conceptual depiction of the layers of the risk protection volume.

4. Uncertainty Modelling

The localization error that must be accounted for in geofence generation is mathematically described in this section.

4.1 Primary Surveillance Radar errors

Radar calculates target location by measuring its range and two angular coordinates with respect to the radar position. The angular coordinates commonly used are the elevation angle that is relative to the local horizontal, and the azimuth measured relative to the true north [10]. A tracking radar has to initially identify the target in space and then determine its range and angular coordinates [11]. Curry [10] summarises the multiple sources that can cause errors in radar measurements as:

- A Signal to Noise (S/N) dependent random measurement error;
- Random measurement error with fixed standard deviation due to noise sources in the radar receiver's final stages. These errors are usually small and correspond to the S/N dependent

errors that are produced when S/N is high;
- A bias error that occurs due to radar calibration and measurement;
- Errors due to conditions of radar propagation and the uncertainties in correcting these errors;
- Interference errors that occur due to various reasons such as radar clutter;

A range measurement error equation is determined based on the major causes of range error [10]:

$$\sigma_R = (\sigma_{RN}^2 + \sigma_{RF}^2 + \sigma_{RB}^2)^{1/2} \quad (4)$$

where σ_{RN} is the S/N dependent random range measurement error, $\sigma_{RN} = \frac{\Delta R}{\sqrt{2\left(\frac{S}{N}\right)}}$ S/N is the signal to noise ratio and ΔR is the Radar Range Resolution ($\Delta R = \frac{c}{2B}$, c is the speed of sound and B is the bandwidth of the signal)

σ_{RF} is the random error with fixed standard deviation produced when S/N is high.

σ_{RB} is the range bias error as a result of calibration and measurement.

Tracking refers to a radar identifying the position of one or more objects in space. Errors also occur when determining the target's azimuth and elevation angles and the requirements determining the accuracy of these angle measurements for a tracking radar are more exacting than those for a search radar [11]. An angular measurement error equation is based on the major causes of angular errors on a radar system:

$$\sigma_A = (\sigma_\omega^2 + \sigma_\varepsilon^2 + \sigma_{EBG}^2)^{1/2} \quad (5)$$

where σ_ω is the rotational error of the radar system occurring due to the jitter of the motor mounted at the base of the radar that enables the rotation of the radar antenna; σ_ε is the error in determining the elevation of the target; σ_{EBG} is the error from the electron beam generated.

4.2 GNSS errors

Various errors affect GNSS positioning, both computed frompseudorange and carrier phase measurements. Sabatini, et al. [12] summarises these errors into the following categories:

- Receiver Dependent Errors such as Clock Error, Noise and Resolution
- Ephemeris Prediction Errors
- Satellite Dependent Errors that includes Clock Offset and Group Delays;
- Propagation Errors such as Ionospheric Delay, Tropospheric Delay and Multipath
- User Dynamics Error

The User Equivalent Range Error (UERE) is a vector alongside the line-of-sight of the user-satellite that is a resultant of the projection of all system errors and is given by the following equation [12]:

$$UERE = \sqrt{(\sigma_{e+cl} + \sigma_{atm} + \sigma_{mp} + \sigma_n)} \quad (6)$$

Where σ_{e+cl} is the broadcast ephemeris and clock error, σ_{atm} is the atmospheric (ionospheric and tropospheric) error, σ_{mp} is the multipath interference and, σ_n is the receiver noise. The GNSS accuracy is not dependent on just the ranging errors, which determines position accuracy, but also on the navigation accuracy that is determined by the relative geometry of the satellites and the user and is given by the Dilution of Precision (DOP) factors [32].

Vertical Dilution of Precision (VDOP)

$$VDOP = \sigma_h \quad (7)$$

Horizontal Dilution of Precision (HDOP)

$$HDOP = \sqrt{\sigma_n^2 + \sigma_e^2} \quad (8)$$

Position Dilution of Precision (PDOP)

$$PDOP = \sqrt{\sigma_n^2 + \sigma_e^2 + \sigma_h^2} \quad (9)$$

Time Dilution of Precision (TDOP)

$$TDOP = \sigma_\tau \quad (10)$$

Where σ_e, σ_n, σ_h are variances of east, north and height components σ_τ is standard deviation in the receiver clock bias. The Estimated Position Error (EPE) and the Estimated Time Errors (ETE) of a GNSS receiver can be calculated using the PDOP (contributing to EPE in 3D), the HDOP (contributing to EPE in 2D) and the TDOP and are given by the following equations [32]:

$$EPE_{3D} = \sigma_R . PDOP \quad (11)$$

$$EPE_{2D} = \sigma_R . HDOP \quad (12)$$

$$ETE = \sigma_R . TDOP \quad (13)$$

Where σR is the standard deviation of pseudo-range measurement error

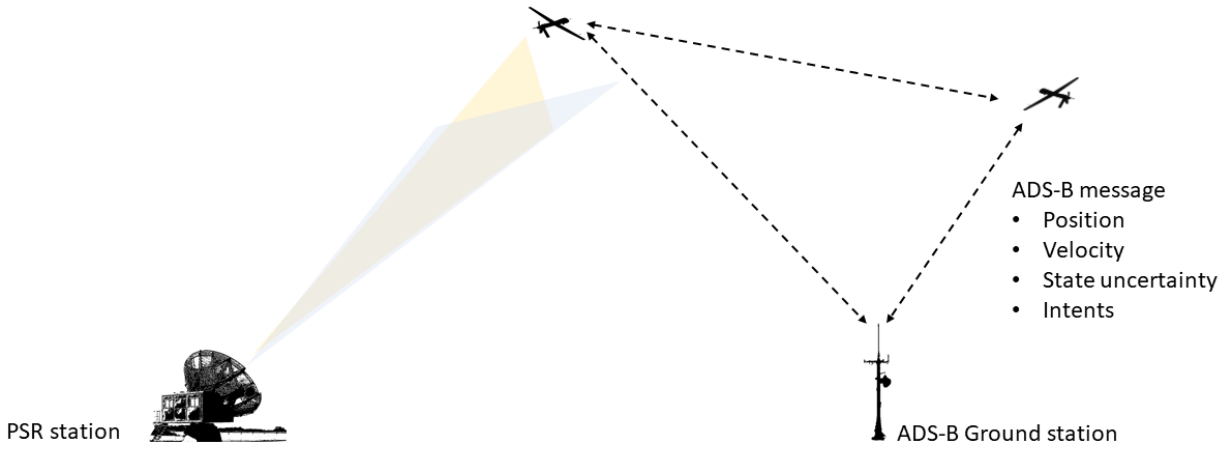

4.3 ADS-B errors

ADS-B is a cooperative surveillance system, wherein aircraft share data through a network. The relevant messages shared via the communication link include aircraft position, velocity, and ID, which are transmitted through a Mode-S Extended Squitter (1090 MHz). This type of scenario is illustrated in Figure 7. As per aviation standards [13], the aircraft position and velocity is obtained from the onboard GNSS receiver. Therefore, the localization component of the error associated with a given ADS-B system is essentially the error affecting the position estimate of the GNSS receiver. In aviation, GNSS-based navigation systems are categorized on the basis of their performance into distinct Required Navigation Performance (RNP) groups, which specify most importantly for the collision risk problem, the accuracy of the computed position solution and its integrity. In addition to the localization error, the latency between when the measurement is made and when it is utilized to assess risk must also be accounted for. ADS-B performance is placed into discrete accuracy and integrity categories. The performance category is part of the broadcast message along with the position and velocity information used to determine potential conflicts. The Navigation Accuracy Category-Position (NACp) specifies the 95% accuracy bounds of the position solution. The Navigation Integrity Category (NIC) specifies the horizontal and vertical integrity containment regions (essentially Protection Levels) as

one of twelve possible integrity categories. These categories and corresponding latency contributions as specified in [14] are summarized in Table 1.

Table 1 - Navigation Integrity Categories and corresponding bounds and latencies

NIC	Horizontal and Vertical Containment Bounds	Latency contribution
0	$R_c \geq$ 37.04 km (20 NM)	1.2 s
1	$R_c <$ 37.04 km (20 NM)	
2	$R_c <$14.816 km (8 NM)	
3	$R_c <$7.408 km (4 NM)	
4	$R_c <$3.704 km (2 NM)	
5	$R_c <$1852 m (1 NM)	
6	$R_c <$1111.2 m (0.6 NM)	
7	$R_c <$370.4 m (0.2 NM)	
8	$R_c <$185.2 m (0.1 NM)	0.4 s
9	$R_c <$ 75 m and VPL< 112 m	
10	$R_c <$ 25 m and VPL< 37.5 m	
11	$R_c <$ 7.5 m and VPL< 11 m	

4.4 Wind forecast uncertainty

In propagating trajectories over time to detect conflicts, it is necessary to account for the non-stationary, inhomogeneous and correlated components of the uncertainty in the wind field. Additionally, uncertainty in wind components at the same location and time of day and season may differ under different weather conditions. Wind forecasts are provided through periodic Numerical Weather Prediction (NWP) models that are accessible to UAS Service Suppliers (USS) through Application Programming Interfaces (APIs). For conflict detection and risk assessment over the online timeframes (5-20 minutes), models such as the HRRR model in the United States is well suited owing to its high frequency data assimilation and update capability. A commonly applied practice in the literature which is also adopted in this paper is to model the wind field as the sum of a nominal and stochastic component. The nominal component is deterministic and is determined from NWP model forecasts that incorporates measurements from radiosondes, aircraft and other sensors. The stochastic component arises due to errors in the model forecast and have typically been determined based on comparison with empirical data, and subsequent extraction of error statistics. Vertical wind components are assumed zero in this work and are to be addressed in future work. Following the approach in [15], the stochastic horizontal components of wind $w(t, P)$ are modelled as a function of time and location:

$$w(t, P): \mathbb{R} \times \mathbb{R}^3 \rightarrow \mathbb{R}^2 \tag{14}$$

These errors are correlated over space (position P) and time t, and prior work has been done in characterizing forecast error statistics. In particular, the Rapid Update Cycle (RUC), the precursor of the HRRR model has been investigated in detail [16]. As documented in [15], $w(t, P)$ is a gaussian random variable with two dimensions (considering horizontal wind fields), and a covariance matrix defined by:

$$R(t, P, t', P') = E[w(t, P)w^T(t', P')] = \begin{bmatrix} r(t, P, t', P') & 0 \\ 0 & r(t, P, t', P') \end{bmatrix} \tag{15}$$

The wind field is assumed isotropic in the horizontal plane with independent components. As a simplifying assumption, the mean wind velocity vector is assumed to be zero and reflects the deterministic wind forecast. Table 2 lists the RUC model error standard deviations for different altitudes which are verified based on wind measurements obtained from ACARS.

Table 2 - Forecast error standard deviation [16], [17]

Pressure (mb)	$\boldsymbol{\sigma(h)}$
900-800	5.01
800-700	4.96
700-600	4.75
600-500	4.48
500-400	4.54
400-300	4.57
300-200	5.17
200-100	5.35

An alternate simplifying assumption is sometimes applied in the literature to ignore the correlation altogether, implying that forecast error standard deviation is constant over the horizontal dimensions and time. If the aircraft is in level flight, then a conservative assumption can be made:

$$r(t, P, t', P') = \sigma^2(h) \tag{16}$$

4.5 Coordinate transformation

In order to combine the different layers into a unified risk volume, the layers must be described in a common coordinate system. Assumed uncertainties for navigation and tracking based on GNSS and Radar are defined as $[\sigma_{X\_GNSS},\ \sigma_{Y\_GNSS},\ \sigma_{Z\_GNSS}]$, $[\sigma_{R\_Radar},\ \sigma_{A\_Radar},\ \sigma_{E\_Radar}]$ respectively. The tracking uncertainty ellipsoid resulting from the azimuth, elevation and range errors is given by the following equations:

$$R_{radar} = R_T + \sigma_R cos\eta cosv \tag{17}$$

$$\alpha_{radar} = \alpha_T + \sigma_\alpha sin\eta cosv \tag{18}$$

$$\varepsilon_{radar} = \varepsilon_T + \sigma_\varepsilon sinv \tag{19}$$

Where r_T, α_T, and ε_T is the position of the detected target in terms of range, azimuth and elevation. The practice employed in this paper will be to transform the radar observations of the host and intruder aircraft to a local cartesian coordinate system. Transformation of this ellipsoid is given by the following equations:

$$X_{T\_radar} = X_{radar} + R_{radar} cos\alpha_{radar} cos\varepsilon_{radar} \tag{20}$$

$$Y_{T\_radar} = Y_{radar} + R_{radar} sin\alpha_{radar} cos\varepsilon_{radar} \tag{21}$$

$$Z_{T\_radar} = Z_{radar} + R_{radar} sin\varepsilon_{radar} \tag{22}$$

Substituting $R_{radar}, \alpha_{radar}, \varepsilon_{radar}$ from the equations above:

$$X_{T\_radar} = X_{radar} + (R_T + \sigma_R cos\eta cosv) \times \cos(\alpha_T + \sigma_\alpha sin\eta cosv) \times \cos(\varepsilon_T + \sigma_\varepsilon sinv) \tag{23}$$

$$Y_{T\_radar} = Y_{radar} + (R_T + \sigma_R cos\eta cosv) \times \sin(\alpha_T + \sigma_\alpha sin\eta cosv) \times \cos(\varepsilon_T + \sigma_\varepsilon sinv) \tag{24}$$

$$Z_{T\_radar} = Z_{radar} + (R_T + \sigma_R cos\eta cosv) \times \sin(\varepsilon_T + \sigma_\varepsilon sinv) \tag{25}$$

Expanding the above equations:

$$X_{T\_radar} = X_{radar} + (R_T + \sigma_R cos\eta cosv)[\cos\alpha_T \cos(\sigma_\alpha sin\eta cosv) . \cos\varepsilon_T \cos(\sigma_\varepsilon sinv) - \cos\alpha_T \cos(\sigma_\alpha sin\eta cosv) . \sin\varepsilon_T \sin(\sigma_\varepsilon sinv) - \sin\alpha_T \sin(\sigma_\alpha sin\eta cosv) . \cos\varepsilon_T \cos(\sigma_\varepsilon sinv) + \sin\alpha_T \sin(\sigma_\alpha sin\eta cosv) . \sin\varepsilon_T \sin(\sigma_\varepsilon sinv)] \quad (26)$$

$$Y_{T\_radar} = Y_{radar} + (R_T + \sigma_R cos\eta cosv)[\sin\alpha_T \cos(\sigma_\alpha sin\eta cosv) . \cos\varepsilon_T \cos(\sigma_\varepsilon sinv) - \sin\alpha_T \cos(\sigma_\alpha sin\eta cosv) . \sin\varepsilon_T \sin(\sigma_\varepsilon sinv) + \cos\alpha_T \sin(\sigma_\alpha sin\eta cosv) . \cos\varepsilon_T \cos(\sigma_\varepsilon sinv) - \cos\alpha_T \sin(\sigma_\alpha sin\eta cosv) . \sin\varepsilon_T \sin(\sigma_\varepsilon sinv)] \quad (27)$$

$$Z_{T\_radar} = Z_{radar} + (R_T + \sigma_R cos\eta cosv)[\sin\varepsilon_T \cos(\sigma_\varepsilon sinv) - \cos\varepsilon_T \sin(\sigma_\varepsilon sinv) \quad (28)$$

Mean error of the tracking error ellipsoid is given by the following equations

$$\mu_{x,Radar} = X_{radar} + \mu_{R,Radar} . cos\mu_{\alpha,Radar} cos\ \mu_{\varepsilon,Radar} \quad (29)$$

$$\mu_{y,Radar} = Y_{radar} + \mu_{R,Radar} . sin\mu_{\alpha,Radar} cos\ \mu_{\varepsilon,Radar} \quad (30)$$

$$\mu_{z,Radar} = Z_{radar} + \mu_{R,Radar} . sin\mu_{\varepsilon,Radar} \quad (31)$$

Assuming the range, azimuth and elevation of the target tracked by the radar as $r_T, \alpha_T, \varepsilon_T$ respectively, the tracking error uncertainty ellipsoid is given by the following equations

$$\sigma_{X\_ellipse\_Radar} = X_{radar} + (R_T + \sigma_R cos\eta cosv)[\cos\alpha_T \cos(\sigma_\alpha sin\eta cosv) . \cos\varepsilon_T \cos(\sigma_\varepsilon sinv) - \cos\alpha_T \cos(\sigma_\alpha sin\eta cosv) . \sin\varepsilon_T \sin(\sigma_\varepsilon sinv) - \sin\alpha_T \sin(\sigma_\alpha sin\eta cosv) . \cos\varepsilon_T \cos(\sigma_\varepsilon sinv) + \sin\alpha_T \sin(\sigma_\alpha sin\eta cosv) . \sin\varepsilon_T \sin(\sigma_\varepsilon sinv)] - X_{radar} - r_T cos\alpha_T cos\varepsilon_T \quad (32)$$

$$\sigma_{Y\_ellipse\_Radar} = Y_{radar} + (R_T + \sigma_R cos\eta cosv)[\sin\alpha_T \cos(\sigma_\alpha sin\eta cosv) . \cos\varepsilon_T \cos(\sigma_\varepsilon sinv) - \sin\alpha_T \cos(\sigma_\alpha sin\eta cosv) . \sin\varepsilon_T \sin(\sigma_\varepsilon sinv) + \cos\alpha_T \sin(\sigma_\alpha sin\eta cosv) . \cos\varepsilon_T \cos(\sigma_\varepsilon sinv) - \cos\alpha_T \sin(\sigma_\alpha sin\eta cosv) . \sin\varepsilon_T \sin(\sigma_\varepsilon sinv)] - Y_{radar} - r_T sin\alpha_T cos\varepsilon_T \quad (33)$$

$$\sigma_{Z\_ellipse\_Radar} = Z_{radar} + (R_T + \sigma_R cos\eta cosv)[\sin\varepsilon_T \cos(\sigma_\varepsilon sinv) - \cos\varepsilon_T \sin(\sigma_\varepsilon sinv)] - Z_{radar} - r_T sin\varepsilon_T \quad (34)$$

Since the rotation transform is non-linear, the Jacobian of the rotation matrix is used. This locally linear approximation of the rotation is performed so as to preserve the Gaussianity of the tracking errors. Considering a GNSS-based navigation system, the navigation uncertainty ellipsoid is given by the following equations which are natively in the cartesian frame:

$$\sigma_{X\_ellipse\_GNSS} = \sigma_{X\_GNSS} cos\eta cosv \quad (35)$$

$$\sigma_{Y\_ellipse\_GNSS} = \sigma_{Y\_GNSS} sin\eta cosv \quad (36)$$

$$\sigma_{Z\_ellipse\_GNSS} = \sigma_{Z\_GNSS} sinv \quad (37)$$

5. Simulation case studies

A UAS encounter scenarios where the surveillance modalities are radar and ADS-B are simulated. In both cases GNSS is used as the navigation sensor on the host UAV. The parameters describing the scenario are summarized in Table 1.

Table 3 – Radar and ADS-B scenario specifications

Radar surveillance	
Operational factors	**Specifications**
Aircraft	Fixed wing UAVs Wingspan: 15 m
Radar parameters	Monostatic scanning Primary Surveillance Radar • σ_R= 4 m • σ_{Az} = 13° • σ_{El} = 26°
Trajectories	Level flight Constant speed and heading Intersecting routes
ADS-B surveillance	
Operational factors	**Specifications**
Aircraft	Fixed wing UAVs Wingspan: 15 m
Navigation	GNSS receiver: GPS • RNP 0.1; Accuracy: 185.2 m • RNP 0.05; Accuracy: 92.6 m
Trajectories	Level flight Constant speed and heading Parallel routes

For the first scenario, the error uncertainty ellipsoids due to Radar and GNSS are plotted in Figure 8, along with the combined dynamic geofence at one epoch.

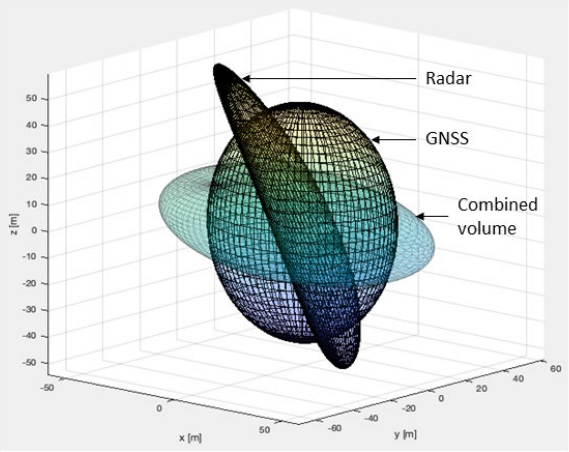

Figure 8 – Combined GNSS and Radar errors

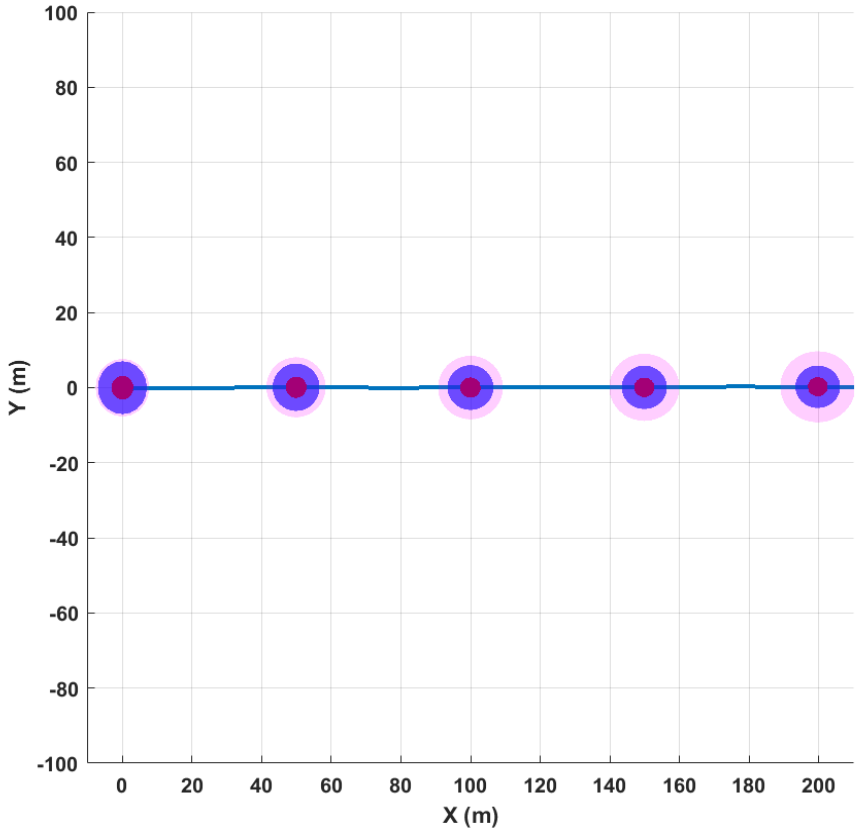

Figure 9 – Navigation (red) and surveillance (blue) volumes, and inflation due to wind uncertainty (magenta)

For the second case, the surveillance modality in this instance is ADS-B. The host and intruder aircraft follow parallel routes, travelling at a level altitude, with a constant speed and heading. The navigation accuracy category of 2σ = 185.2 m is considered. This corresponds to an RNP 0.1 accuracy specification. The altitude of both aircraft is 700 m (corresponding to 800-900 mb pressure). At this altitude, wind uncertainty is assumed constant at a value of 5.01 m/s, based on the data summarized in Table 2. At each epoch, the forecast trajectory is characterized by growing uncertainty over the time horizon due to the uncertainty in the wind forecast.

6. Conclusion

This article presented a flexible DAA analytical approach that accounts for the varying performance of the avionics sensors/systems and ATM ground equipment supporting aircraft flight operations. The model is intended to support the unsegregated access of Unmanned Aircraft Systems (UAS) to all classes of airspace, and the complexities associated with such operations. The relevant navigation, communication and surveillance performance factors were converted to a spatial bound to form a dynamic geofence surrounding each aircraft (the same concept can be easily applied to ground obstacles for low-level flight operations). Various inflation methods developed in previous research were summaries (i.e., relative dynamics, weather and turbulence) where briefly summarized and a new inflation model was introduced in this paper to account for uncertainty in wind forecasts. Future work will further investigate the impacts of communication performance and vehicle dynamics on the collision risk. Additionally, the potential to incorporate factors such as adverse weather and wake turbulence (including that of eVTOL aircraft) as buffer layers in the risk protection volume will be addressed. Furthermore, future work will tackle the application of the model to path planning and trajectory optimization for automated manned and unmanned aircraft collision avoidance tasks.

7. Copyright Statement

8. References

[1] (2020). *Federal Aviation Administration - UTM Concept of Operations v2.0, Department of Transportation, Washington D.C.*

[2] A. G. Gardi, K. de Ridder, R. Sabatini, and S. Ramasamy, "4-Dimensional Trajectory negotiation and validation system for the next generation air traffic management," in *AIAA guidance, navigation, and control (GNC) conference*, 2013, p. 4893.

[3] J. K. Kuchar and L. C. Yang, "A review of conflict detection and resolution modeling methods," *IEEE Transactions on intelligent transportation systems,* vol. 1, no. 4, pp. 179-189, 2000.

[4] J. Tang, "Conflict detection and resolution for civil aviation: A literature survey," *IEEE Aerospace and Electronic Systems Magazine,* vol. 34, no. 10, pp. 20-35, 2019.

[5] R. A. Paielli and H. Erzberger, "Conflict probability estimation for free flight," *Journal of Guidance, Control, and Dynamics,* vol. 20, no. 3, pp. 588-596, 1997.

[6] K. Bilimoria, H. Lee, Z.-H. Mao, and E. Feron, "Comparison of centralized and decentralized conflict resolution strategies for multiple-aircraft problems," in *18th Applied Aerodynamics Conference*, 2000, p. 4268.

[7] Y. Yang, J. Zhang, K.-Q. Cai, and M. Prandini, "Multi-aircraft conflict detection and resolution based on probabilistic reach sets," *IEEE Transactions on Control Systems Technology,* vol. 25, no. 1, pp. 309-316, 2016.

[8] *Minimum Operational Performance Standards (MOPS) for Detect and Avoid (DAA) Systems (DO-365A)*, RTCA, 2020.

[9] M. B. Jamoom, M. Joerger, S. Khanafseh, and B. Pervan, "Unmanned aircraft system sense and avoid integrity and continuity risk for non-cooperatve intruders," in *AIAA Infotech@ Aerospace*, 2015, p. 0484.

[10] G. R. Curry, *Radar system performance modeling*. Artech House, 2005.

[11] H.-J. Li and Y.-W. Kiang, "Radar and inverse scattering," in *The Electrical Engineering Handbook*: Elsevier, 2005, pp. 680-682.

[12] R. Sabatini, T. Moore, and S. Ramasamy, "Global navigation satellite systems performance analysis and augmentation strategies in aviation," *Progress in Aerospace Sciences,* vol. 95, pp. 45-98, 2017.

[13] *Minimum Aviation System Performance Standards For Automatic Dependent Surveillance Broadcast (ADS-B)*, RTCA, Washington, DC 2002.

[14] *DO-242 Minimum Aviation System Performance Standards for Automatic Dependent Surveillance Broadcast (ADS B)*, RTCA, 2006.

[15] W. Glover and J. Lygeros, "A multi-aircraft model for conflict detection and resolution algorithm evaluation," *HYBRIDGE Deliverable D,* vol. 1, no. 3, 2004.

[16] R. Cole, C. Richard, S. Kim, and D. Bailey, "Assessment of the 60 km rapid update cycle (RUC) with near real-time aircraft reports," 1998.

[17] G. Chaloulos and J. Lygeros, "Effect of wind correlation on aircraft conflict probability," *Journal of Guidance, Control, and Dynamics,* vol. 30, no. 6, pp. 1742-1752, 2007.